NASA MEaSUREs: Making Earth System Data Records for Use in Research Environments (NNH06ZDA001N)

An Earth System Data Record for Land Surface Freeze/Thaw State

ALGORITHM THEORETICAL BASIS DOCUMENT (ATBD)

[Version 1]

[1,3]John S. Kimball, [2]Kyle C. McDonald, [3]Youngwook Kim, and [3]Joseph G. Glassy

[1]Flathead Lake Biological Station, The University of Montana
311 Biostation Lane, Polson, MT 59860-9659
Email: johnk@ntsg.umt.edu

[2]Jet Propulsion Laboratory, California Institute of Technology
4800 Oak Grove Drive, Pasadena CA 91109-8099

[3]Numerical Terradynamic Simulation Group (NTSG), The University of Montana, Missoula MT 59812

July 3, 2009

CONTENTS

1. Introduction

This document represents and Algorithm Theoretical Basis Document (ATBD) for developing an Earth System Data Record (ESDR) quantifying global vegetated land surface freeze/thaw state (F/T) dynamics. The freeze/thaw ESDR (FT_ESDR) will be developed using multi-frequency satellite passive and active microwave remote sensing time series spanning multiple missions and sensors, including passive microwave radiometery from the Scanning Multichannel Microwave Radiometer (SMMR), Special Sensor Microwave Imager (SSM/I) and Advanced Microwave Scanning Radiometer for EOS (AMSR-E), and radar scatterometry from SeaWinds-on-QuikSCAT. These records are global in extent and provide a contiguous time series extending from 1979 onward with some overlap between missions.

The science justification, algorithms, calibration, and validation approaches for the FT_ESDR are well established, having been developed from an extensive heritage of past NASA Earth Science research. Satellite microwave remote sensing is uniquely capable of detecting and monitoring a range of related biophysical processes associated with the measurement of landscape F/T status. Major landscape hydrological and ecological processes embracing the remotely-sensed F/T signal include the timing and spatial dynamics of seasonal snowmelt and associated soil thaw, runoff generation and flooding, ice breakup in large rivers and lakes, vegetation growing seasons and net primary production (NPP), and the seasonal switch of the land surface between a net source of atmospheric CO_2 in winter and a terrestrial carbon sink following thawing in spring. Thus the F/T state variable provides a surrogate measure of water mobility in the landscape and the interactions between terrestrial water, carbon, and energy cycles.

Global satellite microwave remote sensing records now span a continuous record exceeding 25 years. These observations involve overlapping time series of multi-platform and multi-sensor measurements at multiple frequencies and polarizations, with systematic, daily repeat global monitoring over time spans encompassing pronounced Earth system changes over the last several decades. Since the early 1980s, atmospheric CO_2 concentrations have increased by more than 40 ppm, largely due to anthropogenic emissions from fossil fuel burning. Earth surface changes coinciding with these perturbations include warming of global annual mean surface air temperatures exceeding 0.4°C, five to thirteen day advances in the onset of seasonal growing seasons, increases in fire frequency and severity, regional shifts in vegetation cover and productivity, and large changes in plant-available moisture and the terrestrial water balance. Current satellite observations are capable of detecting and monitoring many of these changes, though a fundamental challenge for global change assessment and monitoring is that most time-series satellite data were not initially designed for the detection and monitoring of climate change. The precision and temporal stability of these measurements and their ability to quantify long-term biophysical changes is compromised by several factors, including variations in geometric and radiometric precision among instrument time series, and variations in spectral, spatial and temporal resolutions of measurement time series. Nevertheless, retrospective analyses and correction of overlapping sensor time series records can retrieve improved information for diagnosing the trajectories of Earth system changes and their interrelationships.

The requirements of the FT_ESDR are that F/T measurements will be derived over global vegetated land areas where seasonally frozen temperatures are primary environmental constraints to NPP and land-atmosphere exchanges of radiatively active trace gases. The data record will

achieve a F/T spatial resolution of 25-km with mean daily temporal sampling of 3 days or better above 45°N. The data record will be of sufficient duration and accuracy to distinguish landscape F/T characteristics in accordance with episodic mesoscale weather events, annual anomalies, periodic climate cycles and long-term change trajectories encompassed by a global data record spanning up to 25 years or more. The freeze/thaw status of the aggregate vegetation-snow-soil layer will be determined sufficiently to characterize the timing and duration of frozen temperature constraints to vegetation productivity at the scale of individual biomes and resolve mean annual variations in NPP and growing season length to within 3% relative error over relatively homogenous vegetated land areas consistent with moderate (~25-km) resolution global satellite microwave remote sensing observations. These requirements form the basis of the FT_ESDR design. This ATBD includes descriptions of both baseline and optional algorithms and discussion of major theoretical assumptions and procedures for refining and testing FT_ESDR algorithms and outputs in meeting these requirements.

The FT_ESDR will provide a consistent and well calibrated record of the spatial pattern, temporal variability and long-term changes in terrestrial F/T dynamics, enabling accurate assessment of associated changes in terrestrial growing seasons and vegetation productivity, seasonal snow cover, permafrost and land-atmosphere energy, water and carbon exchanges. The enhanced precision and consistent temporal record provided by the FT_ESDR will improve measurement and diagnosis of climate change trajectories and impacts to the global biosphere. Anticipated applications of the FT_ESDR include global change assessment and monitoring, numerical weather forecasting, hydrological and biospheric assessment, and baseline information for future NASA Earth observation missions.

2. Overview and Background

Over one-third (50 million km^2) of the global land mass experiences seasonal F/T processes, affecting surface hydrological activity, surface meteorology and ecological trace gas dynamics profoundly. The conceptualization and biophysical importance of the F/T signal is well established. Abrupt near 0°C, the F/T state transition represents the closest analog to a hydrological and biospheric on/off switch existing in nature, while the relative influence of these processes on terrestrial water, carbon and energy cycles increases with landscape moisture content and at higher latitudes and elevations (Nemani et al. 2003; Running and Kimball 2005).

The F/T signal from satellite microwave remote sensing coincides with arrival of seasonal snow cover in Fall (Frolking et al. 1999; Kimball et al. 2004b); seasonal snowmelt, flooding and the new release of water in the landscape in the spring (Rawlins et al. 2005; McDonald and Kimball 2005); seasonal shifts in land surface albedo and the ratio of sensible and latent energy exchange (Running et al. 1999), and the onset and duration of annual growing seasons for northern ecosystems (Frolking et al., 1999; Kimball et al., 2004b). The timing of snowmelt, soil and foliage thaw has a major impact in determining annual NPP (Jarvis and Linder 2000; Kimball et al. 2004, 2006) and whether an ecosystem is a net annual source or sink for atmospheric CO_2 (Frolking et al. 1996; Goulden et al. 1998, Kimball et al. 2004b). Interannual variability in land-atmosphere CO_2 exchange is caused not only by variability in CO_2 uptake, but also by respiration processes. Changes in the timing and length of the seasonal frozen period as determined from the SSM/I time series coincides with the duration of snow cover and annual variations in the surface energy budget and soil thermal regime (Smith et al. 2004). Interannual

variability in the duration of the annual frozen period as determined from SSM/I and SeaWinds time series also impacts NPP and land-atmosphere CO_2 exchange indirectly by influencing soil decomposition rates and associated release of plant-available N (McDonald et al. 2004; Kimball et al. 2007); these effects are magnified in northern ecosystems and upper elevations where soil decomposition is reduced by low temperatures and vegetation productivity is N limited.

A growing body of evidence indicates that growing seasons, vegetation productivity and land-atmosphere CO_2 exchange patterns are shifting in response to global change-related warming and associated decreases in cold temperature constraints to plant growth (Myneni et al. 1997; Randerson et al. 1999; Nemani et al. 2003; Euskirchen et al. 2006; Kimball et al. 2006). Previous analyses of northern F/T cycles using the SSM/I indicate a significant temporal advance in the timing of spring thaw for the northern latitudes of approximately 4-6 days per decade between 1988 and 2001. (McDonald et al., 2004; Smith et al. 2004). These thaw trends coincided with a similar lengthening of the growing season at high latitudes (Smith et al. 2004; Euskirchen et al. 2006). The timing of the mean SSM/I seasonal thaw signal also corresponded directly with the timing and maximum seasonal drawdown of atmospheric CO_2 from biospheric net photosynthesis, while the timing of thaw for a given year was a significant ($P<0.001$) predictor of the seasonal amplitude of atmospheric CO_2 for the following year. These results were also consistent with satellite remote sensing and prognostic model simulations of recent shifts in vegetation productivity and soil thermal dynamics for northern ecosystems (Myneni et al. 1997, Kimball et al. 2007, Euskirchen et al. 2006). All of these studies indicate a general lengthening of annual growing seasons for northern ecosystems associated with recent warming trends that are well within the temporal extent of the global satellite microwave remote sensing record.

2.1 Product/Algorithm Objectives

The objective of the FT_ESDR is to provide a consistent, systematic long-term global record of land surface F/T state dynamics for vegetated regions where low temperatures are a major constraint to ecosystem processes. The FT_ESDR will be of sufficient duration and accuracy to: 1) distinguish F/T heterogeneity in accordance with mesoscale climate, and landscape topographic and land cover features; 2) establish biophysical linkages between landscape F/T processes and vegetation productivity, respiration and associated land-atmosphere CO_2 exchange; 3) distinguish landscape F/T characteristics in accordance with episodic weather events, annual anomalies, periodic climate cycles and long-term change trajectories encompassed by a global data record spanning up to 25 years or more.

The FT_ESDR will provide time series geospatial information on landscape F/T state dynamics with sufficient accuracy, resolution, and coverage to resolve physical processes linking Earth's water, energy and carbon cycles. To meet these requirements, the F/T status of the aggregate landscape vegetation-snow-soil layer will be determined to a sufficient level to characterize low-temperature constraints to NPP and soil-vegetation-atmosphere exchanges of radiatively active trace gases. The FT_ESDR will have a mean F/T transition temporal fidelity of three days or better and spatial resolution of approximately 25 km, sufficient to resolve mean annual variations in NPP and growing season length to within 3% relative error over relatively homogenous vegetated land areas and individual biomes. Independent calibration and validation approaches using global biophysical station network data archives will be used for F/T algorithm calibration and documentation of relative accuracy of the FT_ESDR time series.

2.2 Historical Perspective

Satellite microwave remote sensing is uniquely capable of detecting and monitoring a range of related biophysical processes associated with the measurement of landscape F/T status (Running et al. 1999, McDonald and Kimball 2005). The ability of microwave sensors to observe freezing and thawing of a landscape has its origin in the distinct changes of surface dielectric properties that occur as water transitions between solid and liquid phases. Consisting of highly polar molecules, liquid water exhibits a dielectric constant that dominates the microwave dielectric response of natural landscapes. As liquid water freezes, the molecules become bound in a crystalline lattice, impeding the free rotation of the polar molecules and reducing the dielectric constant substantially. The large temporal change in landscape dielectric properties associated with the F/T transition dominates the seasonal pattern of radar backscatter and microwave emissions. Major landscape hydrological and ecological processes embracing the remotely-sensed F/T signal include the timing and spatial dynamics of seasonal snowmelt and associated soil thaw, runoff generation and flooding, ice breakup in large rivers and lakes, vegetation growing seasons and productivity, and the seasonal switch of the land surface between a net source of atmospheric CO_2 in winter and a terrestrial carbon sink following thawing in spring.

The scientific requirements for the F/T measurement follow from an extensive heritage of past research, including truck-mounted microwave scatterometer and radiometer studies of bare and sparsely vegetated soils and croplands (Ulaby et al. 1986, Wegmuller 1990), aircraft Synthetic Aperture Radar (SAR) campaigns over forested landscapes (Way et al. 1990), and more recently, a variety of satellite-based SAR, scatterometer and radiometer studies at regional and continental scales (Rignot and Way 1994, Way et al. 1997, Frolking et al. 1999, Kimball et al. 2001, 2004a,b, 2006, McDonald et al. 2004, McDonald and Kimball 2005, Rawlins et al. 2005). Most of these studies exploit the landscape dielectric constant response to F/T state transitions and associated changes in microwave brightness temperature and radar backscatter. This dynamic response dominates the seasonal microwave remote sensing signatures for areas of the globe where F/T processes occur. The F/T signal from satellite microwave sensors is also robust because these sensors can observe the global land surface effectively day or night independent of solar illumination and most atmospheric effects. While continuous coverage of surface F/T state conditions is possible, actual coverage is defined by sensor configuration and orbit design.

2.3. Data Product Characteristics

The FT_ESDR structure will encompass one or more distinct, but related variables depending upon selection of the baseline and optional algorithms. The baseline F/T variables will include consistent global maps of the timing (Julian day) of primary seasonal thaw and freeze events and duration (days) of annual frozen and non-frozen periods, posted to a regular Earth grid. Related F/T variables from optional algorithms include a daily binary freeze/thaw state classification on a grid cell by cell basis. The structure and biophysical significance of these variables have previously been established using SSM/I and SeaWinds sensor data streams over regional and continental extents (e.g., Kimball et al. 2004, 2006, McDonald et al. 2004, Rawlins et al. 2005; Zhang et al. 2008). The global extent of the F/T classifications will encompass unmasked

vegetated land areas where low temperatures are a major constraint to vegetation productivity. Masked areas will include permanent ice and snow, non-vegetated land, open water and regions unconstrained by freezing temperatures. The FT_ESDR map projections will be defined in terms of both polar azimuthal and global cylindrical Equal-Area Scalable Earth (EASE) grids (Armstrong and Brodzik 1995). These gridding schemes are similar to current postings for SSM/I and AMSR-E distributed through the NSIDC DAAC (e.g., http://nsidc.org/data /amsre/data_summaries.html). The FT_ESDR will be posted to a 12.5-km resolution Earth grid, while the native resolutions of the microwave remote sensing data used for F/T classification vary for individual sensors and frequencies, ranging from 5-60 km with overlapping orbital swath data at high latitudes. The FT_ESDR will utilize a nested grid system to facilitate merging and intercomparison of native resolutions for radar backscatter and microwave brightness temperature series. Resampling, interpolation, and reprojection methods will include weighted two-dimensional interpolation of swath sample points falling within a specified radial distance of each grid point, using inverse distance or inverse distance squared interpolation approaches. Resampling approaches will involve one or more of the following: nearest neighbor, bin averaging, and optimal interpolation. Formatting of FT_ESDR products will involve EOSDIS-HDF with appropriate metadata. These metadata will include a dynamic quality-control (QC) index ascribed to the respective time series maps summarizing F/T classification accuracy in relation to in situ surface air temperature measurement networks, and terrain and land cover heterogeneity.

All data processing for the FT_ESDR will occur over unmasked portions of the global domain. No data processing will occur over masked areas, including ocean, open water, and permanent ice and snow. There will be at least four types of "no-data" flags in the final FT_ESDR product series identifying and distinguishing missing data values, ocean, open water, and masked land pixels. The F/T algorithms to be employed for this project are not dependent on ancillary data. However, a variety of ancillary data may be included as a means to enhance algorithm efficiency and accuracy. These products may include a 1-km resolution gridded global mask image indicating land-ocean margins, fractional open water, and permanent ice and snow. These ancillary data are available from established global datasets including MODIS 1-km resolution land cover (http://edcdaac.usgs.gov/modis/mod12q1.asp; Friedl et al. 2002); JERS-1 and SRTM derived fractional open water classifications; SRTM and/or USGS GTOPO30 derived 30-arc second (1-km) resolution topographic slope, aspect and elevation (http://edcdaac.usgs.gov/gtopo30/gtopo30.asp; Row et al. 1995; USGS 1993). These data will be resampled to a consistent geographic projection as the FT_ESDR product. The FT_ESDR will also utilize WMO global surface weather station based daily air temperature information, which are available for up to 5600 mid to high latitude stations through the National Climate Data Center (NCDC); these data will be used for FT_ESDR algorithm calibration and accuracy assessment. The results of these comparisons will be used with terrain and land cover heterogeneity information to define temporally dynamic QC information for the FT_ESDR time series.

3. Physics of the Problem

The ability of microwave remote sensing instruments to observe freezing and thawing of a landscape has its origin in the distinct changes of surface dielectric properties that occur as water transitions between solid and liquid phases. A material's permittivity describes how that material responds in the presence of an electromagnetic field (Kraszewski, 1996). As an electromagnetic field interacts with a dielectric material, the resulting displacement of charged particles from their equilibrium positions gives rise to induced dipoles that respond to the applied field. A material's permittivity is a complex quantity (*i.e.*, having both real and imaginary numerical components) expressed as:

$$\varepsilon = \varepsilon' - j\varepsilon'' \tag{1}$$

and is often normalized to the permittivity of a vacuum (ε_0) and referred to as the relative permittivity, or the *complex dielectric constant*:

$$\varepsilon_r = \varepsilon'/\varepsilon_0 - j\varepsilon''/\varepsilon_0 = \varepsilon_r' - j\varepsilon_r''. \tag{2}$$

The real component of the dielectric constant, ε_r', is related to a material's ability to store electric field energy. The imaginary component of the dielectric constant, ε_r'', is related to the dissipation or energy loss within the material. At microwave wavelengths, the dominant phenomenon contributing to ε_r'' is the polarization of molecules arising from their orientation with the applied field. The dissipation factor, or *loss tangent,* is defined as the ratio:

$$\tan(\delta) = \varepsilon_r''/\varepsilon_r'. \tag{3}$$

Consisting of highly polar molecules, liquid water exhibits a dielectric constant that dominates the microwave dielectric response of natural landscapes (Ulaby *et al*., 1986, pp. 2022-2025). As liquid water freezes, the molecules become bound in a crystalline lattice, impeding the free rotation of the polar molecules and reducing the dielectric constant substantially. In general, landscapes of the terrestrial cryosphere consist of a soil substrate that may be covered by some combination of vegetation and seasonal or permanent snow. The sensitivity of radar and brightness temperature signatures to these landscape features is affected strongly by the sensing wavelength, as well as landscape structure and moisture conditions. The composite remote sensing signature represents a sampling of the aggregate landscape dielectric and structural characteristics, with sensor wavelength having a strong influence on the sensitivity of the remotely sensed signature to the various landscape constituents.

In the microwave region of the electromagnetic spectrum, vegetation canopies may be considered to be weakly scattering media (*i.e.* media characterized by volume absorption that is much larger than volume scattering), with the first-order approximation to canopy scattering being applicable. In this case, diffuse scattering effects may be ignored and first-order scattering model approaches utilized to interpret backscatter (Ulaby *et al*., 1986, vol. II). At higher frequencies, scattering effects of the vegetation are increasingly significant. The dependence of the microwave signatures on vegetation characteristics is complex, with vegetation structure strongly influencing radar signatures.

Radar remote sensing of the total co-polarized backscatter from the landscape at polarization *p* is the sum of three components:

$$\sigma_{pp}^{t} = \sigma_{pp}^{s} \exp(-2\tau_c) + \sigma_{\mathrm{pp}}^{\mathrm{vol}} + \sigma_{pp}^{\mathrm{int}} \tag{4}$$

The first term is the surface backscatter, σ_{pp}^{s}, modified by the two-way attenuation through a vegetation layer of opacity τ_c along the slant path. The second term represents the backscatter from the vegetation volume, σ_{pp}^{vol}. The third term represents interactions between vegetation and the surface, σ_{pp}^{int} (Ulaby *et al*., 1986 vol II, pp. 860-875; Ulaby *et al*., 1990; Kuga *et al*., 1990). The response of σ_{pp}^{t} to freeze/thaw dynamics is affected by surface roughness, topography, and vegetation and snow cover. The relative contribution of the three terms in Equation (5) is influenced strongly by the canopy opacity, τ_c. Opacity and volume scattering vary significantly with frequency. For bare surface or sparsely vegetated conditions, the surface terms dominate the received signal, with σ_{pp}^{t} being influenced primarily by contributions from the soil surface and snow cover. Because of the high dielectric constant of liquid water, microwave penetration of the vegetation decreases as biomass moisture levels increase. In general, τ_c increases with increasing frequency, vegetation density, and dielectric constant. High-frequency, short wavelength energy (*e.g.* Ku-band) has higher τ_c and does not penetrate as significantly into vegetation canopies as lower frequency, longer wavelength energy (*e.g.* L-band). Hence, lower frequency sensors are generally more sensitive to properties of surfaces underlying dense vegetation canopies. However, the dependence of σ_{pp}^{t} on snow characteristics is also complex, with snow pack wetness, density, crystal structure, and depth influencing backscatter. The effect of snow cover on radar backscatter is more significant at higher frequencies owing to the increased scattering albedo of the snow pack at short wavelengths relative to longer wavelengths (*e.g.*, Ulaby *et al*., 1986; Raney, 1998) These phenomena lead to notable differences in the temporal response of emission and backscatter to landscape freeze/thaw processes with sensor wavelengths (*e.g.*, Way *et al*., 1994; Way *et al*., 1997; Frolking *et al*., 1999; Kimball *et al*., 2001).

4. Retrieval Algorithms

Derivation of the FT_ESDR product will employ a temporal change detection approach that has been previously developed and successfully applied using time-series satellite remote sensing radar backscatter and radiometric brightness temperature data from a variety of sensors and spectral wavelengths. The general approach of these techniques is to identify landscape F/T transition sequences by exploiting the dynamic temporal response of backscatter or brightness temperature to differences in the aggregate landscape dielectric constant that occur as the landscape transitions between predominantly frozen and non-frozen conditions. These techniques assume that the large changes in dielectric constant occurring between frozen and non-frozen conditions dominate the corresponding backscatter and brightness temperature temporal dynamics, rather than other potential sources of temporal variability such as changes in canopy structure and biomass or large precipitation events. This assumption is valid during periods of seasonal freeze/thaw transitions for most areas of the cryosphere.

We will utilize up to three distinct temporal change detection algorithms to classify and map landscape F/T state using available global satellite microwave radar and radiometry data records. The F/T algorithms include a seasonal threshold approach representing our baseline algorithm, as well as optional temporal edge detection and moving window algorithms that may be used to augment the current baseline algorithm. These algorithms are described in detail below. All of these algorithms require only time-series radar backscatter or brightness temperature information to derive landscape F/T state information. However, we will utilize ancillary data to enhance

algorithm performance, including the use of digital terrain, land cover and open water classification maps and in situ weather station air temperature measurements to calibrate and refine algorithm parameters and mask open water and permanent ice areas during FT_ESDR data processing (*e.g., see Section 4.4*).

4.1 Seasonal threshold approach (baseline algorithm)

Seasonal threshold approaches examine the time series progression of the remote sensing signature relative to signatures acquired during a seasonal reference state or states. These techniques are well-suited for application to data with temporally sparse or variable repeat-visit observation intervals and have been applied to ERS and JERS Synthetic Aperture Radar (SAR) imagery (*e.g.* Rignot and Way, 1994; Way *et al*., 1997; Gamon *et al*., 2004; Entekabi *et al*., 2004). A seasonal scale factor $\Delta(t)$ may be defined for an observation acquired at time t as:

$$\Delta(t) = \frac{\sigma(t) - \sigma_{fr}}{\sigma_{th} - \sigma_{fr}} \tag{6}$$

where $\sigma(t)$ is the measurement acquired at time t, for which a freeze/thaw classification is sought, and σ_{fr} and σ_{th} are measurements (backscatter or brightness temperature) corresponding to the frozen and thaw reference states, respectively. In situations where only a single reference state is available, for example σ_{fr}, $\Delta(t)$ may be defined as a difference:

$$\Delta(t) = \sigma(t) - \sigma_{fr} \tag{7}$$

A threshold level T is then defined such that:

$$\begin{aligned} \Delta(t) &> T \\ \Delta(t) &\le T \end{aligned} \tag{8}$$

define the frozen and thawed landscape states, respectively. This series of algorithms will be run on a cell-by-cell basis for unmasked portions of the domain. The output from (8) will be a dimensionless binary state variable designating either frozen or thawed condition for each unmasked grid cell. Whereas (6) accounts for differences in the dynamic range of the remote sensing response to F/T transitions driven by variations in land cover, (7) does not scale $\Delta(t)$ to account for the dynamic range in the seasonal response.

The selection of parameter T may be optimized for various land cover conditions and sensor configurations. In situations where the wintertime microwave signature is not dominated by the snow pack volume, for example for radar measurements at lower frequencies (*e.g.* L-band) and where shallow dry snowpacks are common, $\sigma_{fr} < \sigma_{th}$ and $\Delta(t) > T$ defines the thawed state. In situations where the wintertime signature is dominated by the snow pack volume, for example at high frequencies (*e.g.* Ku-band) and where deep, wet snowpacks are common, the microwave seasonal response to landscape freeze/thaw is more complex, and defining the frozen and thawed landscape state in terms of a single threshold may not adequately represent these processes. In some applications, multiple threshold values may be employed to delineate multiple freeze/thaw events occurring during seasonal transitions.

4.2 Temporal edge detection approach (optional algorithm)

Temporal edge detection techniques classify freeze/thaw transitions by identifying predominant step-edges in time series remote sensing data that correspond to F/T transition events. As F/T events induce large temporal changes in landscape dielectric properties that tend to dominate the seasonal time-series response of the microwave radiometric signatures for the terrestrial cryosphere, edge detection approaches are suitable for identification of these events using time-series microwave remote sensing data. These techniques are based on the application of an optimal edge detector for determining edge transitions in noisy signals (Canny, 1986). The timing of a major F/T event is determined from the convolution applied to a time series of backscatter or brightness temperature measurements $\sigma(t)$:

$$CNV(t) = \int_{-\infty}^{\infty} f'(x)\sigma(t-x)dx \tag{9}$$

where $f'(x)$ is the first derivative of a normal (Gaussian) distribution. The occurrence of a step-edge transition is then given by the time when $CNV(t)$ is at a local maximum or minimum. Seasonal transition periods may involve multiple F/T events. This technique accounts for the occurrence of weak edges, or less pronounced F/T events, as well as larger seasonal events indicated by strong edges, and can distinguish the frequencies and relative magnitudes of these events. The variance of the normal distribution may be selected to identify step edges with varying dominance, *i.e.* selection of a large variance identifies more predominant step edges, while narrower variances allow identification and discrimination of less pronounced events. This approach has been applied to daily time series brightness temperatures from the Special Sensor Microwave/Imager (SSM/I) to map primary springtime thaw events annually across the pan-Arctic basin and Alaska (McDonald *et al*. 2004, Kimball et al. 2006, Zhang et al. 2008).

4.3 Moving window approach (optional algorithm)

Moving window techniques classify freeze/thaw transitions based on changes in the radiometric signature relative to the temporally averaged signature computed over a moving window of specified duration. These approaches are useful when applied to temporally consistent data sets consisting of frequent (*e.g.*, daily) observations, and for identifying multiple F/T transition events. For a measurement $\sigma(t)$ acquired at time t, the difference $\delta(t)$ relative to a moving window mean may be defined as

$$\delta(t) = \sigma(t) - \sigma_{av}(t - L \le t_0 \le t - 1) \tag{10}$$

where $\sigma_{av}(t - L \le t_0 \le t - 1)$ is the average measurement (backscatter or brightness temperature) acquired over a window of duration L extending over the time interval $(t - L \le t_0 \le t - 1)$. The difference $\delta(t)$ may be compared to various thresholds, as in Eqs. (7) and **Error! Reference source not found.**, to define the timing of critical F/T transitions. These approaches have been employed using both NSCAT and SeaWinds scatterometer data for a variety of regions (Frolking *et al*., 1999; Kimball *et al*., 2001, 2004a,b; Rawlins *et al*., 2005.)

Principal distinctions in the application of (10) have been the duration *L* of the moving window and the selection of thresholds applied to infer transition events.

4.4 Ancillary Data Requirements

The basis for the satellite remote sensing F/T measurement is the mapping of the spatial and temporal dynamics of land surface F/T state transitions for regions of the globe where cold temperatures are limiting to water mobility and biological processes. The FT_ESDR will include vegetated land areas where seasonally cold temperatures are a significant environmental constraint on land-atmosphere exchanges of water, energy and carbon. **Figure 1** shows the relative importance of low temperature limitations to global mean annual vegetation productivity as derived from the EOS MODIS MOD17 Production Efficiency Model (Running et al. 2004). These results indicate that low temperatures constrain vegetation productivity over approximately 65 percent of the global vegetated land area; these areas are also predominantly located in the Northern Hemisphere above approximately 45°N. Annual vegetation productivity and carbon cycle dynamics in these regions are strongly regulated by seasonal cold temperature constraints to photosynthesis and respiration such that growing seasons are largely limited to spring and summer periods (Nemani et al. 2003). We will utilize surface air temperature data from in situ station networks and corrected model reanalysis products (e.g. Zhang et al. 2007) with vegetation phenology model simulations (Jolly et al. 2005) and satellite remote sensing based vegetation productivity information (Running et al. 2004) to define global land areas where seasonal cold temperatures are a major constraint to ecological processes. These results will define the primary FT_ESDR domain.

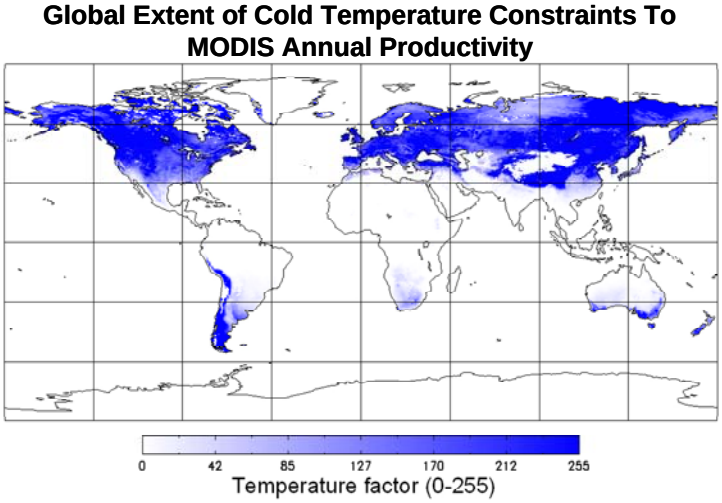

Figure 1. The relative importance of low temperature limitations to global vegetation productivity as derived from the EOS MODIS MOD17 Production Efficiency Model (Running et al., 2004). Low temperatures constrain vegetation productivity over approximately 65 percent of the global vegetated land area. The F/T-ESDR will characterize spatial and temporal dynamics of land surface F/T state transitions for regions of the globe where cold temperatures are limiting to water mobility and biological processes.

The primary input requirement for the FT_ESDR algorithms is time series satellite microwave backscatter or brightness temperature measurements. The F/T classification accuracy is dependent on the wavelength or frequency of microwave measurements, and the spatial resolution and temporal fidelity of the measurements relative to landscape F/T state surface heterogeneity. In general, low to moderate spatial resolution, high temporal revisit microwave radiometers (e.g. SMMR, SSM/I, AMSR-E) and scatterometers (e.g. SeaWinds) are well-suited for quantifying the timing of F/T transitions across broad regions. We will incorporate data from one or more satellite microwave sensors and frequencies to derive the F/T_ESDR. The NASA AMSR-E sensor on the EOS Aqua satellite provides global daily observations since 2002 that are overlapping with ongoing SSM/I and SeaWinds data streams. AMSR-E is a multi-frequency, dual polarization microwave radiometer with a greater number of frequency bands, including longer wavelengths, and with finer native spatial resolution of higher frequency bands than the SSM/I. AMSR-E includes X-band (10.7GHz) and C-band (6.9GHz) wavelengths, which are longer than the lowest SSM/I frequency (19GHz), providing potentially improved resolution of soil, vegetation and snow cover components of the landscape F/T signal (Kim and England 2003; Jones et al., 2007). These attributes enable a larger brightness temperature response to seasonal F/T variations and more precise discrimination and mapping of landscape F/T processes. However, the SSM/I provides a longer time series of potential F/T observations extending from 1988 to present. Reprocessing of overlapping data takes has resulted in enhanced spatial resolution SSM/I and SeaWinds data streams with a relatively high (1-4 day repeat) temporal fidelity (Long and Daum 1998; Early and Long 2001). Application of the spatially enhanced SeaWinds data stream for North America yielded an approximate 4.5km spatial resolution radar backscatter time series that was comparable to MODIS for characterizing the regional vegetation phenology (Frolking et al. 2006). Similar enhanced resolution products are being developed for AMSR-E and provide the potential for additional spatial discrimination of the surface F/T signal.

We will implement one or more approaches for spatial and temporal integration of the SMMR, SSM/I, AMSR-E and SeaWinds data streams into a seamless FT_ESDR. Our baseline approach will involve: 1) processing of individual sensor data streams into distinct global time-series F/T data records; 2) formatting these data into a consistent geographic grid; 3) statistical analyses of the overlapping sensor F/T data series and empirical adjustment and integration of the data into a single, spatially contiguous and temporally consistent long time series F/T record. We have applied similar methods to build long time series vegetation productivity records using NOAA AVHRR and MODIS (e.g., Zhang et al. 2007a,b). These methods are effective and relatively simple to implement, but underutilize potential synergism among alternate sensor frequencies, resolutions and polarizations in determining landscape F/T state. An alternative approach involves a more process-level integration of sensor backscatter and brightness temperatures using a radar backscatter and microwave emissions model framework. Surface land cover and micrometeorological data will be used to simulate multi-frequency radar backscatter and brightness temperatures over a stratified set of surface biosphysical measurement stations representative of major land cover and environmental conditions within the domain. Current radar backscatter and microwave emissions models appropriate to this task include the Michigan Microwave Canopy Scattering (MIMICS) Model (McDonald et al. 1990, 1991, McDonald and Ulaby 1993), and emissivity modeling infrastructure developed in support of NASA SMAP mission risk reduction activities (Kerr and Wigneron 1995, Crow et al. 2005). Backscatter and

emissivity simulation results can then be used to apply algorithms for optimal integration of the various sensor frequencies and polarizations into a continuous time series FT_ESDR.

The F/T algorithms to be employed for this project are not dependent on ancillary data. However, we will examine a variety of potential ancillary data as a means to enhance algorithm efficiency and accuracy. Ancillary data that will be used for FT_ESDR data processing include daily surface meteorological information including global surface weather station network observations. Surface air temperature data from these sites will be used for calibration and refinement of the FT algorithms and validation and documentation of FT_ESDR accuracy. All data processing for the FT_ESDR will occur over unmasked portions of the global domain. No data processing will occur over masked areas, including ocean, open water and permanent ice and snow, as well as areas where low temperatures are not a major constraint to ecosystem processes. There will be at least three types of "no-data" flags in the final FT_ESDR product series identifying and distinguishing ocean, open water, and masked land pixels. Ancillary data used to define the FT_ESDR mask may be obtained from established global datasets including MODIS 1km resolution land cover (http://edcdaac.usgs.gov/modis/mod12q1.asp; Friedl et al. 2002); JERS-1 and SRTM derived fractional open water classifications; SRTM and/or USGS GTOPO30 derived 30-arc second (1km) resolution topographic slope, aspect and elevation (http://edcdaac.usgs.gov/gtopo30/gtopo30.asp; Row et al., 1995; USGS, 1993). These data will be resampled to a consistent spatial scale and geographic projection as the FT_ESDR. We will conduct investigations to set a minimum open water threshold for masking grid cells. The mask image will be a static product for screening satellite microwave data on a grid cell-by-cell basis prior to application of the F/T algorithms. No further F/T data processing will occur for grid cells within masked regions.

4.5 Calibration and Validation

The F/T algorithms are well developed, robust and require little ancillary information for product generation. Production of the FT_ESDR is also feasible given currently available satellite remote sensing products. Global surface biophysical station networks will be used for algorithm calibration and documentation of FT_ESDR product accuracy. The basis for this activity is to refine algorithm coefficients for improved F/T classification accuracy and establish a documented level of spatial and temporal accuracy in the F/T measurement with respect to available measurements from global surface biophysical station networks.

The F/T state characteristics detected by satellite scatterometers and radiometers primarily reflect aggregate surface soil, snow cover and vegetation thermal properties at the spatial resolution of the sensor footprint. Ideally, direct documentation of FT_ESDR time series accuracy requires in situ measurement and spatial extrapolation of landscape component temperatures. Availability of ground-based measurements characterizing thermal regimes for complete landscape component characterization is limited, particularly for high latitudes and elevations because of a general lack of distributed ground based measurements of surface thermal state conditions. We will therefore augment these limited data with surrogate measures of F/T state conditions to extend our data documentation activities over broader regional scales. Optical/IR remote sensing based measurements of surface temperatures are potentially useful, but are also problematic because of sparse coverage and optical image degradation from frequent cloud cover, snow and low solar illumination effects at higher latitudes, particularly during F/T

transition periods. Air temperature provides a useful surrogate of surface F/T state conditions and is readily available in a consistent format from the global surface weather station network. We will follow previously developed F/T validation and documentation protocols using surface weather station networks (e.g. Frolking et al. 1999, McDonald et al. 2004; Rawlins et al. 2005; Kimball et al. 2001, 2004a,b, 2006).

The F/T classification accuracy is sensitive to the selection of temporal compositing window sizes, and frozen and non-frozen reference state conditions. We will apply regional subsets of in situ surface station based air temperatures for F/T algorithm calibration. Spatial heterogeneity in land cover and topography will be evaluated using a 1-km resolution global land cover classification and digital elevation model. This information will be used to select in situ station measurements within regionally homogeneous land areas to ensure regional representation of surface air temperature measurements within relatively coarse (~25km) resolution satellite footprints. The surface air temperature data for each site location will be classified into daily frozen or non-frozen states using simple temperature thresholds. The F/T algorithm coefficients will then be calibrated to maximize temporal agreement (e.g. regression based correlation and significance) and minimize error (RMSE and mean absolute error) and mean residual differences between satellite and station temperature based F/T classification results over the F/T classification domain.

We will apply a 2-tier approach for accuracy assessment and documentation of the FT_ESDR time series using: (1) pixel-to-point comparisons between satellite based F/T classifications and co-located global surface weather station network air temperature measurements over the entire FT_ESDR time-series; (2) Periodic, focused assessments and documentation of FT_ESDR results relative to landscape component temperatures, biophysical measurements, and relatively fine scale remote sensing based F/T results for selected sub-regions.

4.5.1 Tier-1 documentation:

Spatial and temporal assessment of the FT_ESDR time series will be conducted through detailed pixel-to-point comparisons with daily air temperatures from the WMO global surface weather station network. Raw daily temperature data for up to 5600 mid to high latitude stations (> 40°N) are currently used for numerical weather forecasts and are available through the National Climate Data Center (NCDC). These data will be processed for the approximate time periods of FT_ESDR data acquisitions and compared with co-located pixels of geo-referenced F/T maps to quantify the relative agreement between surface air temperature and remote sensing based estimates of F/T state. These results will be summarized as a dynamic quality-control (QC) index ascribed to the respective time series maps and metadata of the FT_ESDR time series. Similar methods have been successfully used for validating SSM/I brightness temperature and NSCAT and SeaWinds scatterometer derived F/T time series across broad boreal/arctic regions of Alaska, Canada and Siberia (Boehnke and Wisman, 1997; Way et al., 1997; Frolking et al. 1999, Kimball et al., 2001, 2004a,b, McDonald et al. 2004). At each sample point, radar backscatter and brightness temperature information reflect an aggregate of surface vegetation, snow and bare soil conditions within an approximate 25-km footprint. While in situ weather station measurements do not provide a direct measure of surface F/T state conditions or spatial variability within the sensor footprint, air temperatures have been found to provide a useful surrogate measure of surface thermal state conditions, particularly for early morning and evening

satellite acquisitions because of predominantly stable atmospheric conditions and minimal surface heating during these periods. These conditions also minimize F/T spatial heterogeneity at the scale of the sensor footprint.

4.5.2 Tier-2 documentation:

Relatively robust, but less frequent and spatially extensive FT_ESDR documentation activities will involve leveraging existing biophysical data archives developed from NASA intensive campaigns, including BOREAS, MODLAND BigFoot and NACP, and other related NASA and NSF funded programs and biophysical data archives. Detailed biophysical data are currently collected and available through the FLUXNET tower site networks distributed across North America, Eurasia and other regions of the globe (e.g., Baldocchi et al., 2008). These data acquisition programs are ongoing and include in situ snow depth, soil temperature and air temperature profile measurements, carbon, water and energy exchange within most of the major global biomes. These data are currently available through existing public data archives (e.g. ORNL-DAAC and FLUXNET online archives) or from individual tower site investigators. Biophysical data are generally acquired at half-hourly intervals and processed using somewhat standardized procedures. These data have also been used extensively in support of EOS remote sensing validation activities. Other useful data archives that may be exploited for F/T documentation activities include USDA SCAN, SNOTEL and RAWS networks, which include detailed daily snow cover, and soil and air temperature information. Data from all of these sources have been successfully used to verify landscape F/T products derived from NSCAT and SeaWinds scatterometers (Frolking et al. 1999; Kimball et al. 2001, 2004a,b), and SSM/I and AMSR-E radiometry (McDonald et al. 2004; Jones et al. 2007).

We will document the relative accuracy of FT_ESDR time series through direct comparisons with relatively fine scale satellite microwave remote sensing based F/T products for selected sub-regions. Time series F/T products have previously been developed using ERS-1/2, Radarsat and JERS-1 for Alaska and the BOREAS region of central Canada (Way et al. 1997, Podest 2006). Similar F/T products are being developed for North America in support of NASA NACP research activities (McDonald PI, Kimball Co-I). These regional F/T products are developed from a variety of satellite SAR imagery with finer spatial resolution (~100m), but coarser temporal fidelity than the proposed FT_ESDR. These study regions encompass large latitudinal and elevation gradients a diverse array of climatic, vegetation and topographic conditions. The enhanced spatial and spectral properties of the SAR data will be used with landcover classifications and topographic complexity maps, and biophysical datasets developed from previous intensive field campaigns and validation activities to document sub-grid scale F/T heterogeneity and associated impacts on the overlying FT_ESDR time series. The results of the Tier-2 validation activities will be incorporated within the FT_ESDR metadata in the form of ancillary global F/T classification accuracy maps and summary documentation.

4.6 Quality Control and Diagnostics

The FT_ESDR product as a whole is highly dimensional, since it encompasses a 2D spatial extent, a temporal extent, a range of contributing instruments (SSM/I, AMSR-E, Seawinds Quikscat, each retrieving information via multiple microwave frequencies), frequencies and frequency combinations, as well as one or more algorithms (e.g. edge detection, seasonal

threshold approaches). Taken together, this dimensionality introduces complexity in how quality-control measures are designed, implemented, and ultimately interpreted by users.

Application users expect and will benefit from several types of product quality metrics associated with the overall FT_ESDR as a whole, as well as with primary F/T variables. Such assessments are routinely used within the context of project-level suitability analyses as well as to help users streamline their workflows. Common user workflows are assumed to involve data-reduction steps. For example, as part of a data-order, users typically consult Quality Control metadata to successively reduce or qualify the volume of data ordered to just the minimum subset required by the given project. Such data filtering occurs at both the granule level (via joint time-space queries), and within a given granule at the pixel region level for 2D spatial products, or time-pixel region for 3D products ordered by time and 2 spatial dimensions.

FT_ESDR product quality is anticipated to be driven by at least two types of influences:

1. Algorithmic (runtime or process basis) quality. These influences stem directly from the computational processes as the algorithms are run.
2. Input data (measurement basis) quality. These influences stem from independent, intrinsic properties of the input data that exist apart from any computational process.

The QA/QC scheme documented in this FT_ESDR ATBD emphasizes assessments from (1) above, while presuming that a higher-level qualification process excludes any grossly unsuitable input data sets. The facets of ESDR product quality most driven by algorithmic influences generally pertain to mechanistic and often deterministic properties of the method of solution itself, through which the conceptual intent is transformed to physical results. Maximizing quality at the algorithmic level involves attention to basic modeling best practices and a faithful translation of the conceptual basis into numeric transformations at each sub-step. This necessarily involves an awareness of how potential boundary or "edge" conditions are addressed when encountered. While it is difficult to foresee all potential boundary conditions an algorithm will be exposed to in its life-cycle, awareness that boundary conditions (or regions) often represent likely problem areas improves both algorithm design and implementation.

As mentioned earlier, the second common contribution to ESDR product quality relates to the independent accuracy and quality of the aggregate input data sources -- the satellite microwave radar and/or radiometry data – as well any ancillary data (assimilated climate data for example) used. Since both of these influences ultimately drive FT_ESDR product quality, outright defects and inadequacies due to either factor, or unanticipated interaction effects, can influence the value to the user provided by otherwise high-quality inputs, and/or an otherwise robust, reliable algorithmic methods.

4.6.1 Distinguishing Quality by Algorithm

F/T outputs will be retrieved using up to three different algorithms, including CNV (temporal edge-detection) and STA (seasonal threshold) approaches. It will be critical for users and producers alike to know which method was used in generating a given pixel-wise F/T value; therefore, a 'lineage' data layer will be populated for each product where pixels were derived from more than a single algorithm. The **ft_lineage** variable will therefore contain a code indicating which algorithm was used to generate the pixel (e.g. 0=CNV and 1=STA, etc…). In the case where a product granule was entirely produced using a single algorithm, a global

NetCDF text attribute (GRANULE_ALGORITHM) will indicate the name of the algorithm (e.g. 'CNV' or 'STA'). If other algorithms are adopted, they will follow this scheme as well.

4.6.2 Granule Level Quality Assurance (QA)

The FT_ESDR data files will be produced using NetCDF version 4.0 following the CF-1.1x conventions for metadata design. The CF conventions are used as a default proxy unless or until a F/T specific convention is devised. In the CF convention, metadata standard names have already been adopted that cover many of the metadata elements we plan to generate, with at least minimal conformance to the existing CF standard and ISO 19116 metadata standard. Simple metadata elements are stored as global attributes in the FT_ESDR product files.

Pertinent to the annual FT_ESDR products, algorithm performance is characterized in terms of the proportion (%) of scene-wise pixels meeting the following quality threshold. A given pixel is considered "accurate" on a given Julian-day when its corresponding climatology pixel minimum temperature is below freezing and its maximum temperature is above freezing. All pixels meeting this quality criteria are placed in a candidate pool (numerator) which is then divided by the total number of pixels evaluated (denominator) to derive a single, scene-wise Percent Accuracy metric. For the daily FT_ESDR product instances, a different methodology is used [TBD].

4.6.3 Pixel Level Quality Assurance Metrics (QA)

The QA/QC approach for assigning pixel level quality metrics is to assign a 4-point categorical score (0=Worst, 1=Poor, 2=Good, 3=Best) on the basis of the performance of the algorithm used to produce the measure. Currently, the default QA implementation is still being refined. The current initial scheme applicable to both the granule and pixel level metrics is summarized in **table 1** below.

Table 1: FT_ESDR Data Product – Initial Pixel and Granule Level QA Scoring Scheme

Pixel QA Categorical score assigned	Criteria (temperatures from assimilated climatology product, in Celsius units)	Comments
3	TBD	Best
2	{Tmax,Tmin >0}, or Tmax,Tmin <0, and {Tavg >= 5 or Tavg <= -5}	Good
1	{Tmax,Tmin >0}, or, { Tmax, Tmin < 0} and {-5 < Tavg < 5}	Poor
0	{Tmax >= 0 and Tmin <= 0}, and {-1 < Tavg < 1.0}, and	Worst

Note that the precise assignment logic for pixel level QA scoring is still being researched at this time.

4.7 Exception Handling

A major contribution to robustness and reliability in any algorithm relates to how exceptions are identified and subsequently handled. In any engineering context, exception handling relates directly to how risk is mitigated for the algorithm and larger processing chain. Exceptions thus represent the "unexpected" and can simplistically occur from:

- An outright (inherent) defect in an individual process input;
- A situational-defect, that is manifest when two (otherwise nominal) process inputs interact in an unexpected way, typically within a processing calculation, or due to an incorrect transformation at a function call-interface;
- An unanticipated behavior within an algorithm when presented with routine (nominal) data (e.g. a rounding error, etc.);
- Encountering an unanticipated boundary or "edge" condition, often expressed via an interaction effect that only manifests when a particular input (mix) is exposed in a particular algorithm region.

As important as identifying an exception as defined above, reliability studies in software engineering have consistently determined that the dynamics of error propagation can be just as important. Several pertinent axioms are:

1. The closer an exception or error is trapped in an algorithm flow-path relative to its origin, the higher the likelihood its effect can be minimized and effectively mitigated;
2. When an exception is allowed (inadvertantly or otherwise) to propagate more deeply through an algorithm flow path, the more likely it is to trigger an error cascade whose discernible symptoms are increasingly disassociated or decoupled from the original error.

4.8 Interface assumptions

4.8.1 High Level FT_ESDR Organization

For the daily product, each granule corresponds to one binary file in NetCDF version 4 format, following the CF 1.1x convention standards for layout. NetCDF recognizes and supports the concepts of "groups" with regard to how data is internally organized and segmented in a given binary file. Each file by default has a 'root' group, present regardless if other user-defined groups are defined. The root group contains all file (granule-level) attributes, called global attributes. The NetCDF CF 1.1x convention dictates a number of global common metadata attributes that will be stored in this root group. FT_ESDR *product specific metadata* will be stored in the "F/T metadata" group as noted below. Additionally, we plan to take advantage of the new NetCDF capability to organize internal data segments by NetCDF "group". Each NetCDF product granule (binary file) will thus consist of at least these high-level encapsulating groups (**Table 2**).

Table 2: FT_ESDR Product, NetCDF Granule level Group Definition

NetCDF internal group	Contains	Form
root	Global attributes and CF	Name value pair, text strings

	conformal metadata	
"F/T metadata"	Product specific metadata	Name value pair text strings, and whole XML
"F/T product_data"	Dimensions and coordinate variables	Dimensions (1D vectors) and coordinate variables (1D vectors with 1 per dimension)
"F/T product_data"	F/T science variable data	Binary frozen or thawed status as documented [TBD]

4.8.2 Nested Grid Definition

A nested grid compatible with similar F/T products and formats from the upcoming SMAP Decadal Survey mission will be used. Nested grid properties applying to the FT_ESDR data products are summarized in **table 3**, noting that all four grids have East-West boundaries at exactly -180.0 and +180.0 longitude.

Table 3: FT_ESDR Data Product Nested Grid Properties

Nominal grid resolution	True resolution at 30 deg latitude	Number of Samples (Columns)	Number of lines (Rows)	No. pixels	Comments
36 km	36.00040003	963	408	393,312	
9 km	9.0001007	3852	1634	6,294,168	
3 km	3.0000336	11556	4904	56,670,624	
1 km	1.0000112	34668	14712	510,035,616	

The current plan is to produce the FT_ESDR data products at least at the 9 km resolution level, for inter-comparison with other ESDR's and ancillary geospatial data products. Projected data volumes thus presume this output resolution, so if others are officially added later, the data volumes will increase accordingly.

4.8.3 Output Product Temporal Granularity

For the annual FT_ESDR product, we are evaluating several different packaging schemes to maximize the usability of the FT_ESDR data:

- Annual granule-file organization. In this organization, the F/T variables (ft_freeze_timing, ft_thaw_timing, ft_freeze_duration, ft_thaw_duration) are stored as 2D gridded measures per

single file.
- Daily granule-file organization. In this layout, the daily repeating F/T variables (ft_state, ft_qa, algor_lineage) are stored as 2D gridded measures per file, with one file produced per Julian day. We are also investigating producing these as (2) biennial files, where data from Julian days {1..180} are stored in one instance, and data from Julian days {181..366} are stored in a second instance file. This will allow users primarily interested in observing a single seasonal "cross-over" from freeze to thaw, or from thaw-to-freeze to work with a smaller easier to work with subset.

Both daily and annual spatio-temporal output products will be produced as part of the FT_ESDR, using the same EASI-Grid nested grid scheme planned for the upcoming SMAP mission, to facilitate inter-comparisons of F/T data with other similar data products. The grid represents a mapping of F/T variables successively nested at 36km, 9km, 3km, and 1km grid resolutions. Note that where native microwave radar or radiometry data is retrieved at a coarser resolution (e.g. 25-60Km for AMSRE and SSM/I), interpolating these data to finer resolutions (9, 3, or 1 km) repetitively maps values at the native (broader) scale to the chosen finer reporting resolution without increasing the geospatial fidelity.

For the daily product, each granule corresponds to one binary file in NetCDF version 4 format. For the annual product, we are evaluating several different packaging schemes to maximize usability of the FT_ESDR data:

- Annual granule-file organization. In this organization, the F/T variables (ft_freeze_timing, ft_thaw_timing, ft_freeze_duration, ft_thaw_duration) are stored as 2D gridded measures per single file;
- Daily granule-file organization. In this layout, the F/T variables (ft_state, ft_qa, algor_lineage) are stored as 2D gridded measures per file, with one file produced per Julian day.

The geospatial extent for the daily and annual products summarized below are identical; processing is limited to terrestrial pixels classified as 'terrestrial' using a cross-walk of all land classes defined in the approved global land-cover dataset (e.g. MOD12Q1 or equivalent), projected on the EASI-Grid using the SMAP nested grid scheme (36km, 9km, 3km, 1km) for regions above 45 degree North (and south) latitude.

The anticipated FT_ESDR data products are outlined in **table 4**, where each product ("F/T State", "F/T Temporal") corresponds to a specific NETCDF file format. Note that for a 9 km output resolution, each variable shown below will be posted to a 3852 x 1634 (6,294,168 total pixels) EASI-Grid projected data layer.

Table 4: FT_ESDR Product Design

Class	Product	Variable (pixel level)	Valid range	Datatype	Comment

Daily	F/T state	ft_state	{0|1|2}, 0=frozen, 1=transition, 2=thawed	Uint8 (byte)	Biophysical state (code)
		ft_qa	{0,1,2,3}, 0=Worst, 1=Poor, 2=Good, 3=Best	Uint8 (byte)	Quality code
		algor_lineage	{0|1|}, 0=CNV method, 1=STA method	Uint8 (byte)	Code indicating which algorithm used
Annual	F/T temporal	freeze_timing	{1..366}	int16	Julian day index
		thaw_timing	{1..366}	int16	Julian day index
		freeze_duration	{1..366}	int16	Count of days in F/T condition
		thaw_duration	{1..366}	int16	Count of days in F/T condition
		ft_qa	{0,1,2,3}: 0=Worst, 1=Poor, 2=Good, 3=Best	Uint8	Quality code.
		algor_lineage	{0|1} 0=CNV, 1=STA	Uint8	Code indicating which algorithm used

4.9 Test Procedures

Test procedures for establishing a level of accuracy and consistency in the FT_ESDR data record are summarized in the Calibration and Validation section above. In addition to these other Cal/Val activities, biophysical measurements from in situ station measurement networks will be used to drive physical models of radar backscatter and microwave emissions within a model sensitivity analysis framework to assess FT_ESDR algorithm and freeze/thaw classification uncertainties in response to uncertainties in sensor retrievals and classification algorithms, and terrain and land cover heterogeneity within the sensor FOV. Detailed error budgets will be derived from these results that define algorithm performance, error sources and associated contributions to FT_ESDR uncertainty.

4.10 Algorithm Baseline Selection

Test procedures and review criteria will be similar for both baseline and optional algorithms. Algorithms not selected for baseline products will be considered research algorithms and will continue to be evaluated after baseline selection. Baseline and optional algorithms will be coded together with ‘switches’ to facilitate algorithm substitution or parallel processing of alternative F/T algorithms and outputs during FT_ESDR development and evaluation. Ancillary data, including surface air temperature measurements, satellite derived NPP products, microwave

emissions and radar backscatter model simulations, ecological phenology model simulations, tower CO2 eddy covariance measurements and atmospheric CO2 concentration measurements compared against F/T results derived from both baseline and optional algorithms. Both baseline and optional algorithm outputs will be complementary, enabling direct comparisons through simple mathematical conversions. We will conduct comparison studies among the various algorithms and evaluate model differences and linkages to field and model based temperature and carbon cycle dynamics to select the most appropriate algorithm as the baseline. Baseline algorithm evaluation and selection will primarily be based on algorithm and product stability and accuracy in meeting FT_ESDR requirements and objectives.

5. Constraints, Limitations, and Assumptions

Expected end uses of the FT_ESDR include regional detection and monitoring of recent (~past 25 years) climate change and associated impacts to ecosystem processes. The F/T status of the aggregate vegetation-snow-soil layer will be determined with sufficient accuracy and precision to characterize the low-temperature constraint to vegetation net primary productivity (NPP) and surface-atmosphere CO_2 exchange. The spatial scale and temporal fidelity of the F/T measurement will be sufficient to resolve the major weather and physiographic elements influencing the surface energy budget and associated F/T heterogeneity at moderate (~25km resolution) spatial scales. These requirements have been found to be sufficient to characterize the temporal dynamics of boreal land-atmosphere CO_2 exchange to within 0.05 tons C ha^{-1} (or 3%) over a ~100-day growing season, and an approximate 1% day^{-1} sensitivity of annual NPP to spring thaw timing for northern and temperate ecosystems (Kimball et al. 2004, 2006). The F/T classification accuracy will be maximized over boreal and Arctic land areas where seasonal frozen temperatures are the dominant constraint to NPP (Nemani et al. 2003), and where land cover and terrain are relatively homogeneous within an approximate 25km sensor field-of-view consistent with available global satellite microwave remote sensing datasets; classification accuracy will be reduced over more complex land cover and topography, and warmer climates.

Several regional and global scale F/T datasets have been developed from a variety of active and passive microwave sensors including the SSM/I, the NASA Scatterometer (NSCAT), SeaWinds and ERS scatterometers; a detailed review of the various algorithms employed, their limitations and assumptions is provided by McDonald and Kimball (2005). The F/T detection algorithms applied to these different sensors all use a temporal change detection classification approach. The FT_ESDR will primarily use available long-term records of existing polar orbiting global satellite microwave sensor observations and will achieve a mean temporal sampling of 3-days or less over northern (>45°N) land areas; temporal sampling of these observations and associated F/T classification accuracy will be reduced at lower latitudes due to diverging polar orbital swaths. Temporal sampling and F/T classification accuracy will also be reduced for areas with frequent, large precipitation events due to data loss from the screening of precipitation events (e.g. Ferraro 1996, Grody and Basist 1996) and erroneous F/T classifications attributed to precipitation induced shifts in radar backscatter and brightness temperatures that may be missed by the precipitation screening process (e.g. Kimball et al. 2004).

The FT_ESDR will be derived from relatively high frequency (e.g., C-band or higher) microwave measurements and moderate to coarse spatial scales that are less sensitive to soil F/T processes and limited in their ability to resolve sub-grid scale heterogeneity. However, these

sensors have demonstrated spatial, temporal and spectral resolutions and accuracies sufficient to characterize annual anomalies and temporal trends in seasonal snowmelt and runoff (e.g. Rawlins et al. 2005), growing season onset and duration (Kimball et al. 2004, 2006), and the seasonal patterns of vegetation productivity and atmospheric CO_2 concentrations (McDonald et al. 2004; Zhang et al. 2008).

6. References

Armstrong, R.L., and M.J. Brodzik, 1995: An Earth-gridded SSM/I data set for cryospheric studies and global change monitoring. *Advances in Space Research*, 16, 155–163.

Baldocchi, D. 2008. Breathing of the terrestrial biosphere: lessons learned from a global network of carbon dioxide flux measurement systems. *Austr. J. Bot.* 56: 1–26.

Baldocchi, D., R. Valentín, S. Running, W. Oechel, and R. Dahlman, 1996. Strategies for measuring and modeling carbon dioxide and water vapour fluxes over terrestrial ecosystems. *Global Change Biology*, 2, 3, 159–168.

Baldocchi, D., E. Falge, L. Gu, et al., 2001. FLUXNET: A new tool to study the temporal and spatial variability of ecosystem-scale carbon dioxide, water vapor, and energy flux densities. *Bulletin of the American Meteorological Society*, 82, 11, 2415.

Boehkne, K., and V. Wismann, 1997. Detecting soil thaw in Siberia with ERS Scatterometer SAR, *Proceedings of the Third ERS Symposium on Space at the Service of our Environment*, Florence, Italy, 17–21 March 1997.

Crow, W.T., S.T.K. Chan, D. Entekhabi, P.R. Houser, A.Y. Hsu, T.J. Jackson, E.G. Njoku, P.E. O'Neill, J. Shi, and X. Zhan, 2005. An observing system simulation experiment for Hydros radiometer-only soil moisture products. *IEEE Trans. Geosci. Rem. Sens*. 43, 6, 1289–1303.

Early, D.S. and D.G. Long, 2001. Image reconstruction and enhanced resolution imaging from irregular samples. *IEEE Trans. Geosci. Rem. Sens.*, 39, 2, 291–302.

Entekhabi, D., E. Njoku, P. Houser, M. Spencer, T. Doiron, J. Smith, R. Girard, S. Belair, W. Crow, T. Jackson, Y. Kerr, J. Kimball, R. Koster, K. McDonald, P. O'Neill, T. Pultz, S. Running, J.C. Shi, E. Wood, and J. Van Zyl, 2004. The Hydrosphere State (HYDROS) mission concept: An Earth System Pathfinder for global mapping of soil moisture and land freeze/thaw. *Transactions in Geoscience and Remote Sensing* 42, 10, 2184–2195.

Euskirchen, E.S., A.D. McGuire, D.W. Kicklighter, Q. Zhuang, J.S. Clein, R.J. Dargaville, D.G. Dye, J.S. Kimball, K.C. McDonald, J.M. Melillo, V.E. Romanovsky, and N.V. Smith, 2006. Importance of recent shifts in soil thermal dynamics on growing season length, productivity, and carbon sequestration in terrestrial high-latitude ecosystems. *Global Change Biology* 12, 731–750.

Ferraro, R.R., 1996. Special sensor microwave imager derived global rainfall estimates for climatological applications. *J. Geophys. Res*. 102(D14), 16,715-16,735.

Friedl, M.A., D.K. McIver, J.C.F. Hodges, et al., 2002. Global land cover mapping from MODIS: Algorithms and early results. *Rem. Sens. Envion.* 83(1–2), 287–302.

Frolking, S., M.L. Goulden, S.C. Wofsy, et al., 1996. Modelling temporal variability in the carbon balance of a spruce/moss boreal forest. *Global Change Biology*, 2, 343–346.

Frolking S., K. McDonald, J. Kimball, R. Zimmermann, J.B. Way and S.W. Running, 1999. Using the space-borne NASA Scatterometer (NSCAT) to determine the frozen and thawed seasons of a boreal landscape. *Journal of Geophysical Research* 104(D22), 27,895–27,907.

Frolking, S., T. Milliman, K. McDonald, J. Kimball, M. Zhao, and M. Fahnestock, 2006. Evaluation of the SeaWinds scatterometer for regional monitoring of vegetation phenology. *Journal of Geophysical Research* 111, D17302, doi:10.1029/2005JD006588.

Goulden, M.L., S.C. Wofsy, J.W. Harden, S.E. Trumbore, P.M. Crill, S.T. Gower, T. Fries, B.C. Daube, S.M. Fan, D.J. Sutton, A. Bazzaz, and J.W. Munger, 1998. Sensitivity of boreal forest carbon balance to soil thaw. *Science*, 279, 214–217.

Grody, N.C., and A.N. Basist, 1996. Global identification of snowcover using SSM/I measurements. *IEEE Trans. Geosci. Rem. Sens*. 34(1), 237-249.

Hansen, M., R. DeFries, J.R. Townshend, M. Carroll, C. Dimiceli, and R. Sohlberg, 2003. Vegetation Continuous Fields MOD44B, 2001 Percent Tree Cover, Collection 3, University of Maryland, College Park, Maryland, 2001.

Jarvis, P. and S. Linder, 2000. Constraints to growth of boreal forests. *Nature* 405, 6789, 904.

Jolly, W.M., R.R. Nemani and S.W. Running, 2005. A generalized, bioclimatic index to predict foliar phenology in response to climate. *Global Change Biology* 11, 619-632.

Jones, L.A., J.S. Kimball, K.C. McDonald, S.K. Chan, E.G., Njoku, and W.C. Oechel. 2007. Satellite microwave remote sensing of boreal and arctic soil temperatures from AMSR-E. *IEEE Transactions on Geoscience and Remote Sensing* 45(7): 2004–2018.

Kerr, Y., and J.-P. Wigneron, 1995. Vegetation models and observations – a review, in Passive Microwave Remote Sensing of Land-Atmosphere Interactions, B. Choudhury, Y. Kerr, E. Njoku, and P. Pampaloni, Eds. Utrecht, The Netherlands: VSP.

Kimball, J.S., K.C. McDonald, S. Frolking and S.W. Running. 2004a. Radar remote sensing of the spring thaw transition across a boreal landscape. *Remote Sensing of Environment* 89(2), 163–175.

Kimball, J.S., K. McDonald, A.R. Keyser, S. Frolking and S.W. Running, 2001. Application of the NASA Scatterometer (NSCAT) for determining the daily frozen and non-frozen landscape of Alaska. *Remote Sensing of Environment* 75, 113–126.

Kimball, J.S., K.C. McDonald, S.W. Running, and S. Frolking, 2004b. Satellite radar remote sensing of seasonal growing seasons for boreal and subalpine evergreen forests. *Remote Sensing of Environment* 90, 243–258.

Kimball, J.S., K.C. McDonald, and M. Zhao, 2006. Spring thaw and its effect on terrestrial vegetation productivity in the western Arctic observed from satellite microwave and optical remote sensing. *Earth Interactions* 10, 21, 1–22.

Kimball, J.S., M. Zhao, A.D. McGuire, F.A. Heinsch, J. Clein, M. Calef, W.M. Jolly, S. Kang, S.E. Euskirchen, K.C. McDonald, and S.W. Running, 2006. Recent climate driven increases in vegetation productivity for the Western Arctic: Evidence of an acceleration of the northern terrestrial carbon cycle. *Earth Interactions* 11, 4, 1–23.

Kimball, J.S., A.R. Keyser, S.W. Running, and S.S. Saatchi, 2000. Regional assessment of boreal forest productivity using an ecological process model and remote sensing parameter maps. *Tree Physiology* 20, 761–775.

Kim, E.J., and A.W. England, 2003. A yearlong comparison of plot-scale and satellite footpring-scale 19 and 37 GHz brightness of the Alaskan North Slope. *J. Geophys. Res.* 108(D13), 4388–4404.

Long D.G., and D.L. Daum, 1998. Spatial resolution enhancement of SSM/I data. *IEEE Trans. on Geosci. and Rem. Sen*. 36, 2, 407–417.

McDonald, K.C., J.S. Kimball, E. Njoku, R. Zimmermann, and M. Zhao, 2004. Variability in springtime thaw in the terrestrial high latitudes: Monitoring a major control on the biospheric assimilation of atmospheric CO_2 with spaceborne microwave remote sensing. *Earth Interactions* 8, 20, 1–23.

McDonald, K.C, and J.S. Kimball, 2005. Hydrological application of remote sensing: Freeze-thaw states using both active and passive microwave sensors. Encyclopedia of Hydrological Sciences. Part 5. Remote Sensing. M.G. Anderson and J.J. McDonnell (Eds.), John Wiley & Sons Ltd. DOI: 10.1002/0470848944.hsa059a.

McDonald, K.C., M.C. Dobson, and F.T. Ulaby, 1990. Using MIMICS to Model L-band Multi-angle and Multi-temporal Backscatter from a Walnut Orchard. *IEEE Transactions on Geoscience and Remote Sensing*, 28, 4 , pp. 477–491.

McDonald, K.C., 1991. Modeling microwave backscatter from tree canopies. PhD dissertation, The University of Michigan, Ann Arbor, Michigan, USA.

McDonald, K.C., and F.T. Ulaby, 1993. Radiative transfer modeling of discontinuous tree canopies at microwave frequencies. *International Journal of Remote Sensing* 14, 11, 2097–2128.

Myneni, R.B., C.D. Keeling, C.J. Tucker, G. Asrar, and R.R. Nemani, 1997. Increased plant growth in the northern high latitudes from 1981–1991. *Nature* 386, 698702.

Nemani, R.R., C.D. Keeling, H. Hashimoto, W.M. Jolly, S.C. Piper, C.J. Tucker, R.B. Myneni, and S.W. Running. 2003. Climate-driven increases in global terrestrial net primary production from 1982 to 1999. *Science* 300, 1560–1563.

National Research Council (NRC), 2007. Earth Science and Applications from Space: National Imperatives for the Next Decade and Beyond (Executive Summary), http://www.nap.edu/catalog/11820.html. National Academy of Sciences, National Academies Press, Washington DC, 35 pp.

Podest, E.V., 2006. Monitoring Boreal Landscape Freeze/Thaw Transitions with Spaceborne Microwave Remote Sensing. PhD thesis. University of Dundee, Scotland.

Randerson J.T., C.B. Field, I.Y. Fung, and P.P. Tans, 1999. Increases in early season ecosystem uptake explain recent changes in the seasonal cycle of atmospheric CO2 at high northern latitudes. *Geophysical Research Letters*, 26, 17, 2765–2768.

Rawlins, M.A., K.C. McDonald, S. Frolking, R.B. Lammers, M. Fahnestock, J.S. Kimball, and C.J. Vorosmarty, 2005. Remote sensing of snow at the pan-Arctic scale using the SeaWinds scatterometer. *Journal of Hydrology,* 312, 294–311.

Rignot E., and J.B. Way, 1994. Monitoring freeze-thaw cycles along north-south Alaskan transects using ERS-1 SAR, *Remote Sensing of Environment*, 49, 131–137.

Row, L.W., D.A. Hastings, and P.K. Dunbar, 1995. TerrainBase Worldwide Digital Terrain Data - Documentation Manual, CD-ROM Release 1.0. National Geophysical Data Center, Boulder, Colorado.

Running, S.W., and J.S. Kimball, 2005. Satellite-based analysis of ecological controls for land-surface evaporation resistance. Encyclopedia of Hydrological Sciences. Part 9, Ecological and Hydrological Interactions. M.G. Anderson and J.J. McDonnell (Eds.), John Wiley & Sons Ltd. DOI: 10.1002/0470848944.hsal10.

Running, S.W., J.B. Way, K. McDonald, J.S. Kimball, A.R. Keyser, S. Frolking, and R. Zimmermann, 1999. Recent advances in the use of satellite radar data to monitor freeze/thaw transitions in boreal regions. *Eos,* 80, 19, 213–221.

Running, S.W., R.R. Nemani, F.A. Heinsch, M. Zhao, M. Reeves, and H. Hashimoto, 2004. A continuous satellite-derived measure of global terrestrial primary production. *Bioscience*, 54, 6, 547–560.

Smith N.V., S.S. Saatchi, and J.T. Randerson, 2004. Trends in high northern latitude soil freeze and thaw cycles from 1988 to 2002. *J. Geophysical Research-Atmospheres* 109 (D12): D12101.

Ulaby, F.T., R.K. Moore, and A.K. Fung, 1986. *Microwave Remote Sensing: Active and Passive, Vol. 1–3*, Artec House:Dedham MA.

USGS, 1993. Digital Elevation Models: Data Users Guide 5, Reston Virginia, 38 pp.

Way, J. B., J. Paris, E. Kasischke, E., et al., 1990. The effect of changing environmental conditions on microwave signatures of forest ecosystems: preliminary results of the March 1988 Alaskan aircraft SAR experiment. *Int. J. Remote Sensing*, 11, 1119–1144

Way, J.B., R. Zimmerman, E. Rignot, K.C. McDonald, and R. Oren, 1997. Winter and spring thaw as observed with imaging radar at BOREAS. *J. Geophys. Res.*, 102(D24), 29673–29684.

Wegmuller, U., 1990. The effect of freezing and thawing on the microwave signatures of bare soil, *Remote Sens. Environ.* 33, 123–135.

Zhang, K., J.S. Kimball, E.H. Hogg, M. Zhao, W.C. Oechel, J.J. Cassano and S.W. Running, 2008. Satellite-based model detection of recent climate driven changes in northern high latitude vegetation productivity. *J. Geophys. Res.* 113, G03033, doi:101029/2007JG000621.

Zhang, K., J.S. Kimball, M. Zhao, W.C. Oechel, J. Cassano, and S.W. Running, 2007. Sensitivity of pan-Arctic terrestrial net primary productivity simulations to daily surface meteorology from NCEP/NCAR and ERA-40 Reanalyses. *J. Geophys. Res. - Biogeosciences* 112, G01011, 1–14, doi:10.1029/2006JG000249.

APPENDIX 1: GLOSSARY

[**Adapted from**: Earth Observing System Data and Information System (EOSDIS) Glossary http://www-v0ims.gsfc.nasa.gov/v0ims/DOCUMENTATION/GLOS-ACR/glossary.of.terms.html.]

ALGORITHM. (1) Software delivered by a science investigator to be used as the primary tool in the generation of science products. The term includes executable code, source code, job control scripts, as well as documentation. (2) A prescription for the calculation of a quantity; used to derive geophysical properties from observations and to facilitate calculation of state variables in models.

ANCILLARY DATA. Data other than instrument data required to perform an instrument's data processing. They include orbit data, attitude data, time information, spacecraft engineering data, calibration data, data quality information, data from other instruments (spaceborne, airborne, ground-based) and models.

BROWSE. A representation of a data set or data granule used to pre-screen data as an aid to selection prior to ordering. A data set, typically of limited size and resolution, created to rapidly provide an understanding of the type and quality of available full resolution data sets. It may also enable the selection of intervals for further processing or analysis of physical events. For example, a browse image

might be a reduced resolution version of a single channel from a multi-channel instrument. Note: Full resolution data sets may be browsed.

BROWSE DATA PRODUCT. Subsets of a larger data set, generated for the purpose of allowing rapid interrogation (i.e., browse) of the larger data set by a potential user. For example, the browse product for an image data set with multiple spectral bands and moderate spatial resolution might be an image in two spectral channels, at a degraded spatial resolution. The form of browse data is generally unique for each type of data set and depends on the nature of the data and the criteria used for data selection within the relevant scientific disciplines.

CALIBRATION. (1) The activities involved in adjusting an instrument to be intrinsically accurate, either before or after launch (i.e., "instrument calibration"). (2) The process of collecting instrument characterization information (scale, offset, nonlinearity, operational, and environmental effects), using either laboratory standards, field standards, or modeling, which is used to interpret instrument measurements (i.e., "data calibration").

CALIBRATION DATA. The collection of data required to perform calibration of the instrument science and engineering data, and the spacecraft or platform engineering data. It includes pre-flight calibrator measurements, calibration equation coefficients derived from calibration software routines, and ground truth data that are to be used in the data calibration processing routine.

CORRELATIVE DATA. Scientific data from other sources used in the interpretation or validation of instrument data products, e.g. ground truth data and/or data products of other instruments. These data are not utilized for processing instrument data.

DATA PRODUCT. A collection (1 or more) of parameters packaged with associated ancillary and labeling data. Uniformly processed and formatted. Typically uniform temporal and spatial resolution. (Often the collection of data distributed by a data center or subsetted by a data center for distribution.) There are two types of data products:

DISTRIBUTED ACTIVE ARCHIVE CENTER (DAAC). An EOSDIS facility that archives, and distributes data products, and related information. An EOSDIS DAAC is managed by an institution such as a NASA field center or a university, under terms of an agreement with NASA. Each DAAC contains functional elements for archiving and disseminating data, and for user services and information management. Other (non-NASA) agencies may share management and funding responsibilities for the active archives under terms of agreements negotiated with NASA.

GRANULE. The smallest aggregation of data which is independently managed (i,e., described, inventoried, retrievable). Granules may be managed as logical granules and/or physical granules.

GUIDE. A detailed description of a number of data sets and related entities, containing information suitable for making a determination of the nature of each data set and its potential usefulness for a specific application.

INSTRUMENT DATA. Data specifically associated with the instrument, either because they were generated by the instrument or included in data packets identifed with that instrument. These data consist of instrument science and engineering data, and possible ancillary data.

METADATA. (1) Information about a data set which is provided by the data supplier or the generating algorithm and which provides a description of the content, format, and utility of the data set. Metadata provide criteria which may be used to select data for a particular scientific investigation. (2)

Information describing a data set, including data user guide, descriptions of the data set in directories, and inventories, and any additional information required to define the relationships among these.

NEAR REAL-TIME DATA. Data from the source that are available for use within a time that is short in comparison to important time scales in the phenomena being studied.

ORBIT DATA. Data that represent spacecraft locations. Orbit (or ephemeris) data include: Geodetic latitude, longitude and height above an adopted reference ellipsoid (or distance from the center of mass of the Earth); a corresponding statement about the accuracy of the position and the corresponding time of the position (including the time system); some accuracy requirements may be hundreds of meters while other may be a few centimeters.

PARAMETER. A measurable or derived variable represented by the data (e.g. air temperature, snow depth, relative humidity.

QUICK-LOOK DATA. Data available for examination within a short time of receipt, where completeness of processing is sacrificed to achieve rapid availability.

RAW DATA. Numerical values representing the direct observations output by a measuring instrument transmitted as a bit stream in the order they were obtained. (Also see DATA PRODUCT LEVEL.)

REAL-TIME DATA. Data that are acquired and transmitted immediately to the ground (as opposed to playback data). Delay is limited to the actual time (propagation delays) required to transmit the data.

SPACECRAFT ENGINEERING DATA. Data produced by the engineering sensor(s) of a spacecraft that are used to determine the physical state of the spacecraft, in order to operate it or monitor its health.